Materials Chemistry and Physics 305 (2023) 127979

Contents lists available at ScienceDirect

Materials Chemistry and Physics

journal homepage: www.elsevier.com/locate/matchemphys

Biogenic synthesis of copper oxide (CuO) NPs exploiting *Averrhoa carambola* leaf extract and its potential antibacterial activity

Trissa Saha [a], Mashrafi Bin Mobarak [b,*], Md Najem Uddin [c], Md Saiful Quddus [b], Mustafizur Rahman Naim [d], Nigar Sultana Pinky [b]

[a] Institute of Fuel Research and Development (IFRD), Bangladesh Council of Scientific and Industrial Research (BCSIR), Dhaka, 1205, Bangladesh
[b] Institute of Glass and Ceramic Research and Testing (IGCRT), Bangladesh Council of Scientific and Industrial Research (BCSIR), Dhaka, 1205, Bangladesh
[c] BCSIR Laboratories Dhaka, Bangladesh Council of Scientific and Industrial Research (BCSIR), Dhaka, 1205, Bangladesh
[d] Biomedical and Toxicological Research Institute (BTRI), Bangladesh Council of Scientific and Industrial Research (BCSIR), Dhaka, 1205, Bangladesh

HIGHLIGHTS

- CuO NPs was synthesized exploiting *Averrhoa carambola* leaf extract.
- XRD, XPS, FESEM, EDX, DLS, UV–Vis, Zeta potential analysis was done for characterization.
- XRD, XPS and SPR spectra confirmed the formation of CuO NPs.
- Particle size was measured by using DLS technique and imageJ software based on FESEM image.
- CuO NPs showed sublime antibacterial activity against both gram positive and gram negative bacteria.

GRAPHICAL ABSTRACT

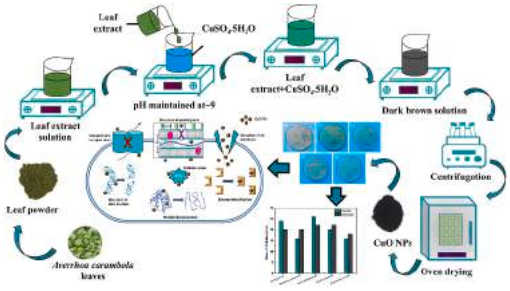

ARTICLE INFO

Keywords:
Green synthesis
Plant extract
Copper (II) oxide
Nanoparticles
Antimicrobial activity

ABSTRACT

Herein, we report our assiduous endeavor to meet one of the demands of 21st century, the green route of synthesis, for copper (II) oxide nanoparticles (CuO NPs) using *Averrhoa carambola* leaf extract for the first time. The synthesized CuO NPs was characterized by XRD, XPS, FESEM, FTIR, DLS, zeta (ζ)-potential and UV–Vis spectroscopic techniques. XRD revealed the monoclinic crystalline phase of the CuO NPs with crystallite size of 24.84 nm. XPS confirmed the surface elemental composition and Cu^{2+} oxidation state of CuO NPs. The formation of NPs was confirmed by the surface plasmon resonance (SPR) spectra based on the sharp absorption at 220 nm. FESEM images showed assorted shapes albeit spherical shapes were the dominant ones. The calculative particle size based on the FESEM images was 98 ± 26 nm whereas DLS analysis showed larger particle size (117 nm) because of hydrodynamic volume. Zeta-potential of the synthesized CuO NPs was found to be −13.65 mV at neutral pH. FTIR analysis confirmed the presence of metal-oxide (Cu–O) bond. The synthesized CuO NPs were exploited as an antibacterial agent against 2 gram positive (*Bacillus megaterium* and *Staphylococcus aureus*) and 3 gram negative bacteria (*Escherichia coli*, *Salmonella typhi and Pseudomonas aeruginosa*). *Salmonella typhi* and *Escherichia coli* were found to be highly vulnerable to CuO NPs with the highest zone of inhibition of 26 mm and 24 mm respectively. Bioresource based green synthesized CuO can be a potential candidate in the array of nanomedicine considering its fascinating activity against broad spectrum bacterial strains.

* Corresponding author.
E-mail address: mashrafibinmobarak@gmail.com (M. Bin Mobarak).

https://doi.org/10.1016/j.matchemphys.2023.127979
Received 18 January 2023; Received in revised form 13 May 2023; Accepted 21 May 2023
Available online 22 May 2023

1. Introduction

Resistance to antimicrobial agents of pathogenic microorganisms (bacteria, fungi, viruses) over the years has become a concernment because of which evolution of new antimicrobial materials is a must [1,2]. Antibiotic misuse has been the leading cause of multidrug resistance in several bacterial strains [3]. A number of diversified bacteria manifest antibiotic resistance via distinct ways like reducing the activity of drug degradation enzyme, altering membrane permeability, altering genetic material (DNA), biofilm forming defensive mechanism along with multi-drug efflux pump developments and results in lower bioavailability of therapeutic drugs in the site of action [4–6]. Therefore, extensive propagation of gram positive and gram negative bacteria exhibits multidrug resistance to broad spectrum antibiotics like penicillin, cephalosporin etc. which are the major categorized beta lactam drug [7]. Subsequently, conventional antibiotic concentrations become inadequate at the site of action which enables increasing antibiotic doses and frequencies of administration associated with more detrimental effects and poor patient compliance. Hence, drug delivery systems are targeted to shoot up the antibacterial potency of available conventional antibiotics [3,8].

Since the last few decades, nanomaterials have attained interest in designing antimicrobial agents and enabled researchers to boost up a way to begin where conventional antibiotics failed to work [9]. Such antimicrobial agents can be of organic or inorganic origin where the inorganic antibacterial materials exhibit good chemical and physical properties with less hazardous effect to human health and environmental pollution [10]. Nanobiotechnology has made things easier by designing inorganic nanoparticles particularly for antimicrobial purposes [11] where they show their activity by disrupting the cell membrane of organism and thus preventing the formation of drug-resistant bacteria. The use of metal nanoparticles i.e., Ag, Au, Ti, Cu, Zn as antimicrobial agents is well established and have been used for centuries [2,12]. There have been an upsurge of literatures that reports the antimicrobial activity of metal oxide nanoparticles, mostly of CuO [13], ZnO [14], TiO_2 [15], Ag_2O [16], Al_2O_3 [17], Fe_2O_3 [18], NiO [19], CaO [20], MgO [21], CoO [22] and SiO_2 [23] NPs.

Among these metal oxide NPs, CuO NPs has attained noteworthy significance in current years due to their multidisciplinary applications such as catalysis [24], heat transfer operations [25], steam reforming [26], CO oxidation of automobile exhaust gases [27], photocathodes for photoelectrochemical water splitting application [28], catalysts for the water-gas shift reaction [29], gas sensors [30], anti-tumor [31], anti-microbial, anti-oxidant and drug delivery agent in biomedicine [32] etc. CuO is a p-type semiconductor which is abundant in nature as starting material with low production cost and its nontoxic behavior [33]. Several synthesis procedures such as reverse microemulsion, solution combustion, thermal decomposition, hydrothermal and thermal oxidation, chemical and sonchemical etc. are being followed for synthesizing CuO NPs. Alternative ways of synthesis are in demand since these methods involve hazardous chemicals, cost ineffectiveness and non-environment friendliness [34]. Moreover, energy crisis and intricate challenges of physical and chemical approaches embolden researchers to unearth substituted possibilities [35].

Bio-resource based green synthesis is one possible solution of such limitations because of eco-friendliness, less toxicity and ease of adaptation according to myriad number of researchers [36,37]. This technique either utilizes micro-organisms (bacteria, fungus, algae etc.) or plant extracts (fruit, leaf, flower, seed etc.) for synthesizing CuO NPs where the later has attained much consideration due to simplicity and ease of implementation [35,38]. Plant extracts in particular contain assorted functional molecules such as phenol, ketones, amides, carboxylic acids, aldehydes, terpenoids, enzymes and flavones which help in reducing the precursor material into CuO NPs as well as stabilizing the NPs [39]. Literatures reported a large number of synthesis procedures of CuO NPs using leaf extract such as *Ruellia tuberosa* [38], *Drypetes sepiaria* [40], *Nerium oleander* [41], *Aloe Vera* [42], *Ixiro coccinea* [43] and *Eucalyptus Globulus* [44] etc. Furthermore, CuO NPs have been evidenced to demonstrate enhanced antibacterial activity against both pathogenic Gram positive and Gram negative bacterial strains such as *Staphylococcus aureus*, *Enterococcus faecalis*, *Klebsiella pneumonia*, *Proteus vulgaris*, *Salmonella typhi*, *Pseudomonas aeruginosa*, *Escherichia coli* and *Bacillus subtilis* etc. [45].

Here in our work, we have synthesized CuO NPs utilizing leaves of *Averrhoa carambola* as capping and reducing agent. *Averrhoa carambola* belongs to the family of Oxalidaceae and extensively cultivated in the South-East Asian Region where commonly known as Kamranga [46,47]. *Averrhoa carambola* contains different types of phytochemicals such as saponins, alkaloids, flavonoids, tannins, antioxidants, proanthocyanidins and L-ascorbic acid etc. [48]. The *Averrhoa carambola* mediated synthesized CuO NPs was investigated for antibacterial activity following the well diffusion method against 2 gram positive (*Bacillus megaterium* and *Staphylococcus aureus*) and 3 gram negative bacteria (*Escherichia coli*, *Salmonella typhi and Pseudomonas aeruginosa*).

2. Materials and methods

2.1. Materials

The precursor, copper sulfate pentahydrate ($CuSO_4.5H_2O$) was procured from Merck, India and sodium hydroxide (NaOH) used in pH adjustment was bought from Scharlau Chemies S.A. All the other chemicals (analytical grade) were used in the experiment without further purification. De-ionized (DI) water was used to prepare solutions in all experiments. Matured *Averrhoa carambola* leaves were collected from the local area of Bisnopur, Magura, Bangladesh on July 2022.

2.2. Methods

2.2.1. Preparation of leaf extract solution

At the very beginning, *Averrhoa carambola* leaves were washed thoroughly with tap water to remove the adherent dirt followed by rinsing with DI water. Then the leaves were sun dried for 72 h and then subjected to grinding for making powder which eased its storing at an air tight container in desiccators. For preparing stock extract solution, 5 g of leaf powder was mixed with 80 ml DI water and heated to 60 °C for 60 min in a 500 ml beaker. After cooling down to room temperature, the slurry was filtered through whatman-1 filter paper and the collected filtrate was stored in 4 °C until further use. This extract solution was used within 7 days of preparation.

2.2.2. Synthesis of CuO NPs

20 g $CuSO_4.5H_2O$ was dissolved in 100 ml DI water in which 10 ml leaf extract was added. The pH of the solution was adjusted to 9 by adding NaOH. The mixture was then subjected to heating at 80 °C and stirring was maintained at 400 rpm for 60 min. The completion of the reaction was visually observed by tracking the change of color of the solution from initial bluish green to brownish black within 60 min, indicating the formation of CuO Nps. After cooling down to room temperature, the solution was centrifuged at 5000 rpm for 10 min and filtered. Remaining residue was collected and washed several times with DI water followed by absolute ethanol. After washing several times, the residual solid CuO NPs was dried in an oven at 60 °C for 5 h. The synthesis scheme of *Averrhoa carambola* extract mediated CuO NPs is shown in Fig. 1.

2.2.3. Characterization of CuO NPs

The phase confirmation of *Averrhoa carambola* extract mediated synthesized CuO NPs was carried out using Rigaku Smart Lab X-ray powder diffractometer. The XRD pattern was recorded within the 2θ range of 30–70° (fixing step 0.01°, scanning rate 30°/min, voltage 40 kV and current 50 mA). Bragg–Brentano para-focusing geometry was used

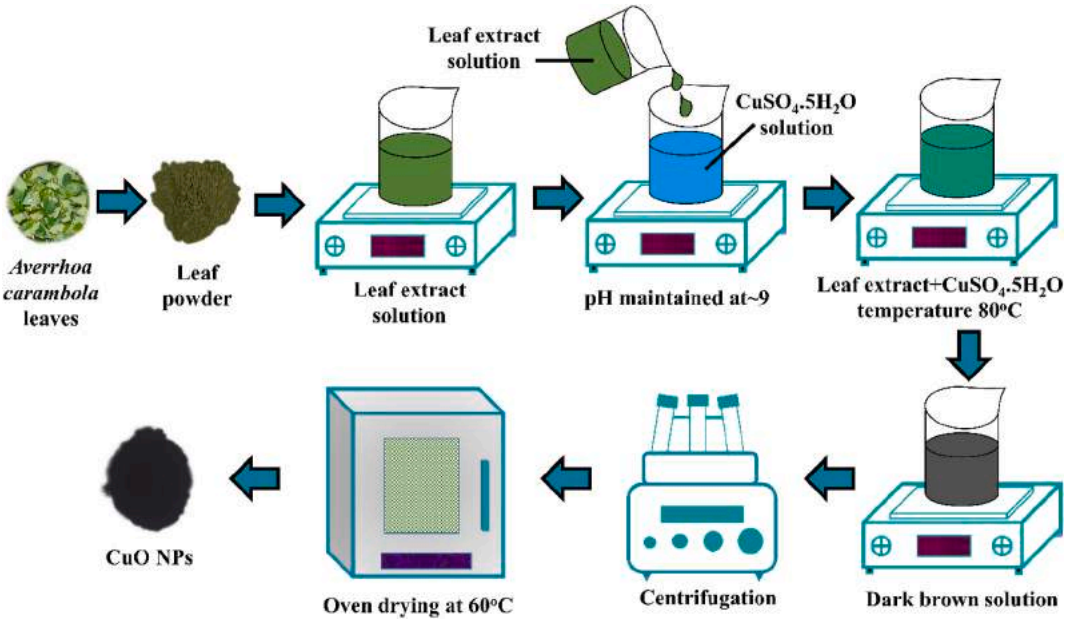

Fig. 1. Synthesis scheme of *Averrhoa carambola* extract mediated CuO NPs.

in recording the data. Matching of the XRD pattern was done with X'Pert highscore plus software with ICDD database.

X-ray photoelectron spectroscopy (XPS) was employed for the elemental confirmation and oxidation state of the elements present in the synthesized CuO NPs, using K-Alpha XPS machine (Thermo Scientific). The machine utilized monochromatic Al Kα radiation which has maximum energy up to 1486.69 eV. The ATR-FTIR (Attenuated Total Reflectance-Fourier Transform Infrared) spectroscopic analysis was done with MIRacle-10 ATR mounted IR Prestige-21 (Shimadzu Corporation, Japan). The wavenumber range was 400-4000 cm^{-1} with resolution of 4 cm and number of scans were 30.

Particle size and zeta potential was measured using a DLS (dynamic light scattering) particle size analyzer (Malvern Panalytical Zetasizer Ultra). To lessen agglomeration, the powdered CuO NPs sample was finely dispersed in ethanol and sonicated for 30min before the analysis. Field emission scanning electron microscopic (JEOL JSM-7610F) images were captured for morphological study of the CuO NPs. The optical properties of CuO NPs was analyzed by dispersing fine CuO NPs particles into absolute ethanol by sonication then taking measurements using Hitachi U-2910 UV–Vis spectrophotometer.

2.2.4. Antibacterial activity study

The antibacterial activity study of the synthesized CuO NPs was carried out against *Escherichia coli* (ATCC 11303), *Pseudomonas aeruginosa* (ATCC 39327), *Salmonella typhi* (ATCC 13311), *Staphylococcus aureus* (ATCC 9144) and *Bacillus megaterium* (ATCC 9885). All these bacterial strains were purchased from American Type Culture Collection (ATCC, Manassas, USA). The antibacterial activity was determined by agar well diffusion method reported elsewhere [49]. Prior to the experiments, bacterial colonies were cultured overnight in Mueller–Hinton Broth (MHB) in a shaking incubator (120 rpm at 37 °C ±2 °C). The cultured colonies were then diluted up to 1:100 with fresh MHB and cultured until it complied the 0.5 McFarland turbidity standards. The 0.5 McFarland turbid suspensions of bacteria were again diluted up to1:1000 to attain 1 × 105 CFU/ml.

2.2.5. Agar well diffusion assay

All the glassware and related accessories for this experiment were autoclaved (temperature 121 °C, pressure 115lb) beforehand. To prepare the agar media, 4.6 g Mueller–Hinton (MH) agar (Oxoid, UK) powder was dissolved in 200 mL DI water and autoclaved. After autoclaving, the MH media was allowed to cool down to around 40 °C after which 50 μL of bacterial colonies were added to the media. This media was then poured into agar plates. Two wells with diameter of 6 mm were created aseptically using sterile micropipette tips on each agar plate after solidifying the media. 50 μL of synthesized CuO NPs with a concentration of 100 μg/mL was loaded in one of the MH agar wells. Other well was loaded with dimethyl sulfoxide (DMSO) (5%) as a negative control. 30 μg disk of Kanamycin was placed on the surface of the media as the positive control. The plates were then kept at 4 °C for 3 h, allowing the penetration and diffusion of nanoparticles through the well, followed by incubation at 37 °C. After 24 h of incubation, clear zones also known as zone of inhibition were found around the wells and the diameter of these zones measured using a slide caliper.

2.2.6. Minimum inhibitory concentrations (MICs)

MIC of the synthesized CuO NPs were performed by standard broth dilution method (CLSI M07-A8) reported elsewhere [50,51]. Briefly, two fold serial dilutions were done for CuO NPs with Brain Heart Infusion (BHI) broth for MIC determination. Five concentrations of CuO NPs: 6.25 μg/mL, 12.5 μg/mL, 25 μg/mL, 50 μg/mL and 100 μg/mL were studied against a bacterial concentration of 1 × 10^5 CFU/ml. In screw cap test tubes, BHI broth containing bacterial strain was used as positive control and the only broth was used as negative control. All the tubes containing considered samples were incubated for 24 h at 37 °C. MIC was determined by visual inspection of the turbidity of the samples before and after incubation.

2.2.7. Minimum bactericidal concentrations (MBCs)

The procedure for MBC study was analogous to MIC study with pintsized addition. After visual determination of MIC, 2 ml BHI broth media was added in each tube and incubated again for 24 h at 37 °C. After incubation, 50 μL sample was withdrawn from the tubes which did not show any bacterial growth and placed in BHI agar plates for culture (incubation at 37 °C for 24 h) and observation of bacterial growth [50, 51].

3. Results and discussion

3.1. X-ray powder diffraction study

The XRD pattern shown in Fig. 2 depicts the orientation and

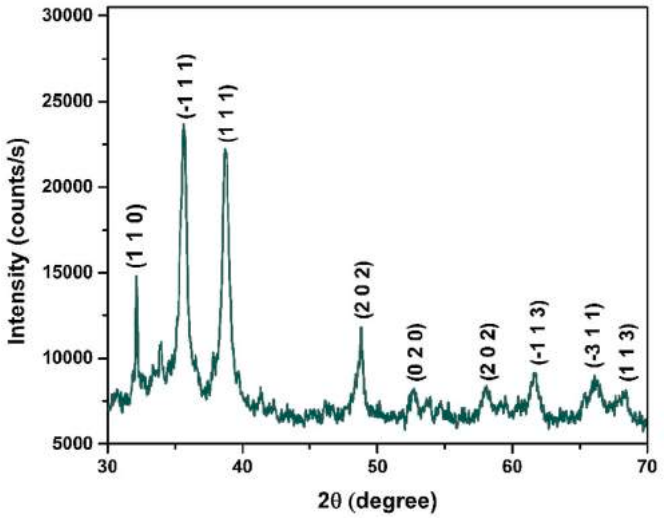

Fig. 2. XRD powder diffraction pattern of synthesized CuO NPs.

crystalline structure of the *Averrhoa carambola* L. extract mediated green synthesized CuO NPS. The pattern shows a series of diffraction peaks at 2θ angles of 32.15°, 35.64°, 38.69°, 48.81°, 52.72°, 58.10°, 61.72°, 66.08° and 68.40° which corresponds to the (110), (−111), (111), (202), (020), (202), (−113), (−311) and (113) crystal planes respectively. Such findings are in harmony with the previous literatures [34,52,53]. The pattern has the best match with the ICDD (International Centre for Diffraction Data) card no #01-080-1268 [54,55]. The presence of two sharpest peaks within the 2θ diffraction angle of 35° and 39° confirms the formation of monoclinic structured CuO NPs [44].

The crystallite size (D) of a material can be defined as the coherent volume for the respective diffraction peak which is also termed as grain size for powdered materials. Crystallite size of the synthesized CuO NPs can be calculated using the widely accepted Scherrer formula, shown in equation (1) [56,57],

$$D = \frac{k\lambda}{\beta \cos\theta} \tag{1}$$

Here, λ is the wavelength of the incident X-Ray beam (0.154060 nm), K is a constant which is usually referred to the broadening constant and is equal to 0.9, β is the full width half maxima (FWHM) in radians and θ is the diffraction angle in degrees.

The crystallographic parameters (unit cell lengths, volume of unit cell and density) were calculated using the following equations (2)–(4) [58],

$$\frac{1}{d^2} = \frac{1}{Sin^2\,\beta}\left(\frac{h^2}{a^2} + \frac{k^2\,Sin^2\,\beta}{b^2} + \frac{l^2}{c^2} - \frac{2hlcos\beta}{ac}\right) \tag{2}$$

$$V = abc\,\sin\beta \tag{3}$$

$$d = \sum \frac{A}{N \times V} \tag{4}$$

Here, V, N and A are volume of unit cell, Avogadro's number ($6.02214076 \times 10^{23} mol^{-1}$) and sum of atomic weight of all the atoms belonging to the unit cell respectively. Equation (4) represents the density of monoclinic structure and for CuO which has 4 molecules in the primitive structure, equation (4) can be written as the following equation (5),

$$d_{CuO} = \sum \frac{4 \times M}{N \times abc\,\sin\beta} \tag{5}$$

Here, M is the molecular weight of CuO ($79.545 gmol^{-1}$). The micro-strain (ε) and dislocation density (δ) of the CuO monoclinic structure can be calculated from the following equations (6) and (7) respectively [58,59],

$$\varepsilon = \frac{\beta}{4\tan\theta} \tag{6}$$

$$\delta = \frac{1}{(D)^2} \tag{7}$$

The calculated results of crystallographic parameters have been compared with the standard values (from ICDD card no #01-080-1268) and presented in Table 1.

3.2. XPS analysis

The elemental confirmation and oxidation state of the elements present in the *Averrhoa carambola* extract mediated green synthesized CuO NPs were carried out in terms of XPS analysis. Fig. 3a shows the survey spectra which confirmed the presence of Cu and O as elements. Trace amount of Na and S were also detected which may have been incorporated from NaOH (used for pH adjustments) and the precursor material $CuSO_4.5H_2O$ respectively. Narrow scan for selected elements i.e., Cu 2p, O 1s and C 1s were also carried out which are shown in Fig. 3 (b–d).

The presence of Cu as an elemental constituent of CuO rather than Cu_2O or metallic Cu was confirmed by the detection of shake-up satellite peaks upon narrow scan of Cu 2p as shown in Fig. 3b. Two shake-up satellite peaks were observed at the higher binding energy sites of the Cu $2p_{3/2}$ peak as well as increased binding energy was observed for the main peak. This indicates the presence of an unfilled *Cu* $3d^9$ shell which also confirmed the Cu^{2+} oxidation state of CuO NPs [60]. The peaks at 952.58 and 932.75 eV (Fig. 3b) correspond to the characteristic Cu $2p_{1/2}$ and Cu $2p_{3/2}$ of Cu^{2+} oxidation state of CuO NPs, also reported in previous literatures [61–63]. The duplet separation of binding energy between Cu $2p_{1/2}$ and Cu $2p_{3/2}$ was 19.83eV, which is also characteristic for CuO nano-structure [63,64].

The core level narrow scan spectra of O 1s is shown in Fig. 3c. The deconvolution of asymmetric core level 1s spectra of O resulted in two peaks at 529.91 and 531.51 eV positions, indicating the existence of two different types of oxygen on the CuO NPs surface. The peak at 529.91 eV corresponded to the oxygen from metal-oxygen bond, in this case the bond between O^{2-} and Cu^{2+} ions of monoclinic CuO [62]. The more intense peak was observed at 531.51 eV position which can be assigned to the surface adsorbed oxygen or the oxygen originated from the phytochemicals of *Averrhoa carambola* extract that acted as the reducing as well as the stabilizing agent [65].

The narrow scanned spectra of C 1s is shown in Fig. 3d. The deconvoluted peak observed at 284.81, 286.32 and 288.51 eV can be assigned to the C–C, C–O–C and O–C═O bond respectively. These peaks can be corresponded to either as adventitious carbon contamination or

Table 1
Lattice parameters (experimental and ICDD values), micro-strain and dislocation density of the synthesized CuO NPs.

Lattice Parameters	a (Å)	b (Å)	c (Å)	Volume of Unit Cell V, $(Å)^3$	Crystal density, d_{CuO} (g/cm^3)	Micro-strain, ε $\times 10^{-2}$	dislocation density, δ $\times 10^{-4}\ nm^{-1}$	Crystallite size, D nm
Experimental values	4.72	3.47	4.92	79.58	6.64	26.13	16.21	24.84
ICDD values (Card No #01-080-1268)	4.68	3.42	5.13	81.03	6.52	–	–	–

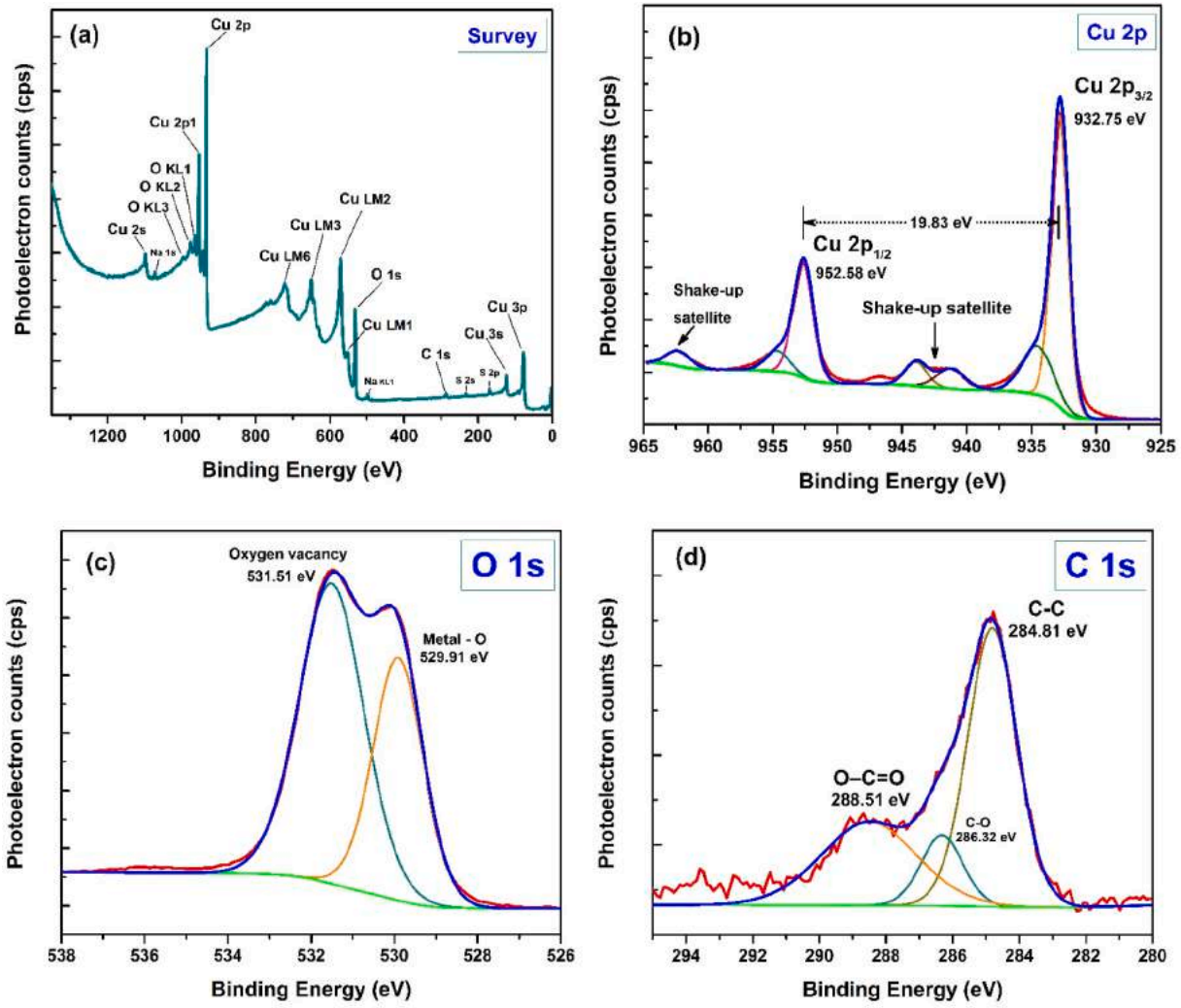

Fig. 3. XPS spectra of *Averrhoa carambola* extract mediated green synthesized CuO NPs (a) survey, (b) Cu 2p, (c) O 1s and (d) C 1s spectra. (For interpretation of the references to color in this figure legend, the reader is referred to the Web version of this article.)

the carbon sources originated from the leaf extract [62,66,67]. The adventitious carbon peak of 284.81 eV was used as a reference peak for the correction of binding energy [66].

3.3. FESEM and EDX analysis

The *Averrhoa carambola* L. extract mediated synthesized CuO NPs have been found to be spherical, oval and irregular shaped (Fig. 4 a and b) under electron microscope where spherical shapes are the most dominant ones, also reported in previous literature [68]. The formation of larger particles (100–170 nm) are due to the agglomeration of the smaller particles which also made the structures irregular shaped. There was no presence of any sort of chunks which eliminated the possibility of extract overuse. Based on the FESEM image, the particle size was measured using imageJ software following the previously reported process [58]. Only the particles that aren't agglomerated and have visible edges were under consideration. The particle size histogram in Fig. 4 (c) shows the average particle size to be of 98 ± 26 nm. For further insights into the elemental composition of the synthesized CuO NPs, the EDX spectra was recorded at 5.0 kV. The peaks appeared for Cu and O corresponded to Cu Lα and O Kα. Negligible peaks were disregarded in the spectra such as carbon and platinum that appears due to the carbon tape adhering the sample to the stub and from conducting coating of the sample respectively. The resultant weight and atom % of Cu was 74.06% and 41.83% whereas O has weight and atom % of 25.94% and 58.17% respectively. The EDX spectra and elemental % has been shown in Fig. 4 (d).

3.4. ATR-FTIR analysis

The ATR-FTIR analysis of the *Averrhoa carambola* L. extract and synthesized CuO NPs were carried out to confirm the presence of functional groups. The spectra were recorded within the wavenumber range of 400-4000 cm^{-1} and have been shown in Fig. 5. ATR-FTIR spectra of both extract and CuO NPs show peak at 3307 and 3390 cm^{-1} and can be assigned to the –OH stretching vibrations which can either be from the phenolic groups of extract or the moisture since nanoparticles are prone to absorb moisture from the environment. Two adjacent bands at 2920 and 2852 cm^{-1} were observed for the extract (Fig. 5a) can be assigned to the –CH and -CH2 stretching vibrations of primary alkanes which was also found at 2985 and 2899 cm^{-1} for the CuO NPs (Fig. 5b) [69–71]. The C═O and N–H bond vibrational bands appeared at 1618 cm^{-1} for the extract and 1636 cm^{-1} for CuO NPs. The vibrational bands at 1436, 1369, 1319 and 1246 cm^{-1} correspond to the C–N stretching and –OH bending vibrations which also indicate the presence of flavonoids and reducing sugars on *Averrhoa carambola* L. extract [72]. Sharp peak at 1039 and 1085 cm^{-1} corresponds to the C–O stretching bands of the carboxylic and phenolic groups [73]. Usually, the vibrational bands for

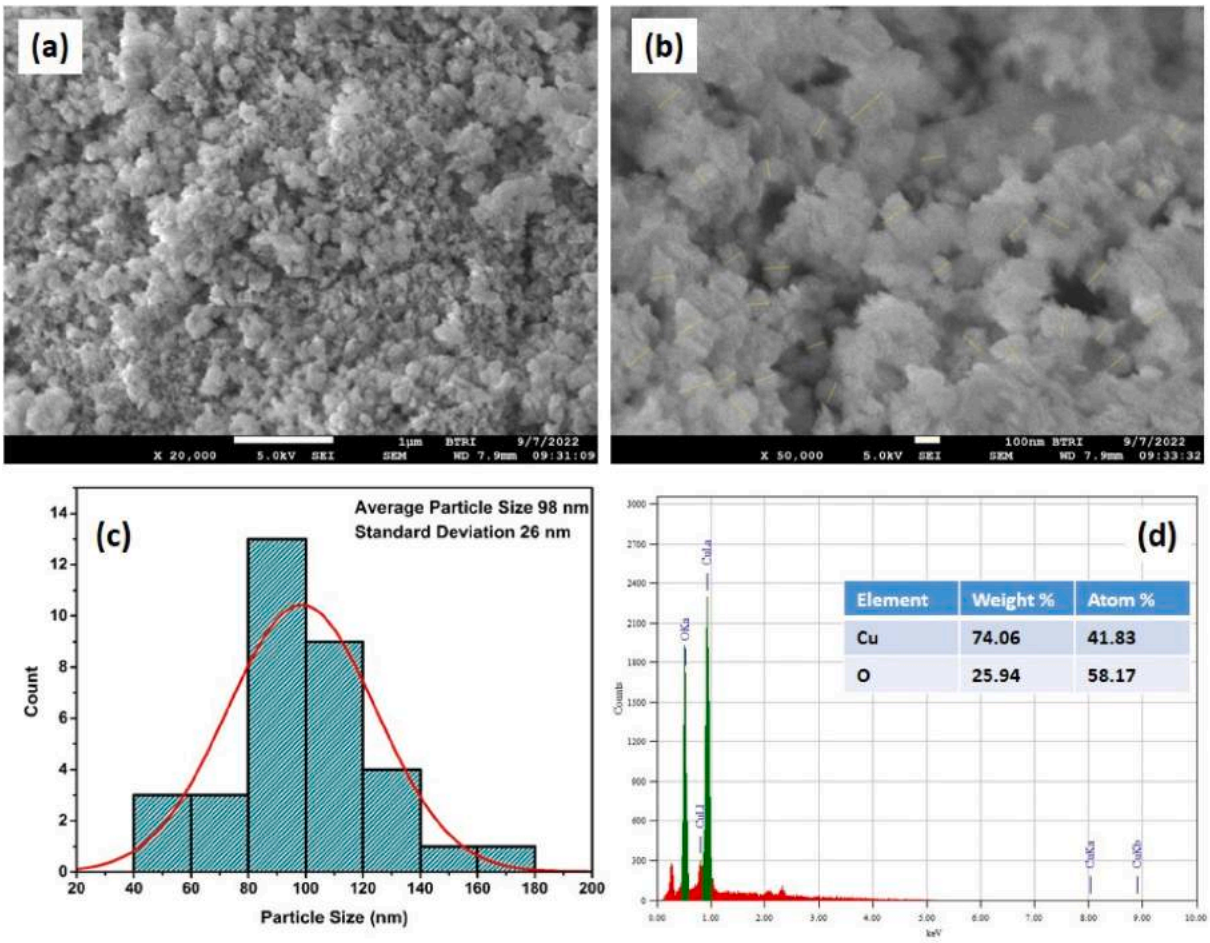

Fig. 4. (a and b) FESEM images of synthesized CuO NPs, (c) Calculated particle size histogram (d) EDX spectra with weight and atom %.

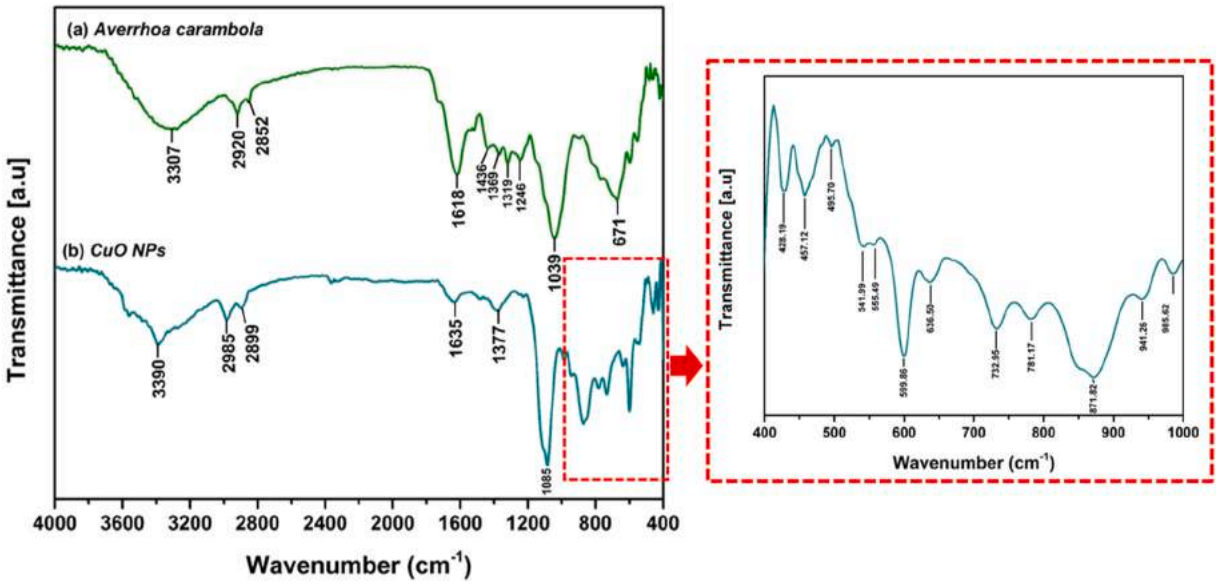

Fig. 5. FTIR spectra of (a) *Averrhoa carambola* L. extract and (b) synthesized CuO NPs.

metal-oxygen bonds are observed under 1000 cm^{-1} region. The bands at 428, 457, 495, 541, 555, 599, 636, 732 and 781 cm^{-1} corresponds to the Cu–O bond of the synthesized CuO NPs [34,44,52,53,58,68,69,74,75]. According to the prediction of group theory, the IR active modes of monoclinic CuO structure are $3A_u+3B_u$ which involves the motion of both Cu and O atoms [75,76]. The bands at 428 and 599 cm^{-1} can be assigned to the A_u and B_u modes respectively which are also the characteristic peaks for monoclinic structured CuO NPs [69]. There were no

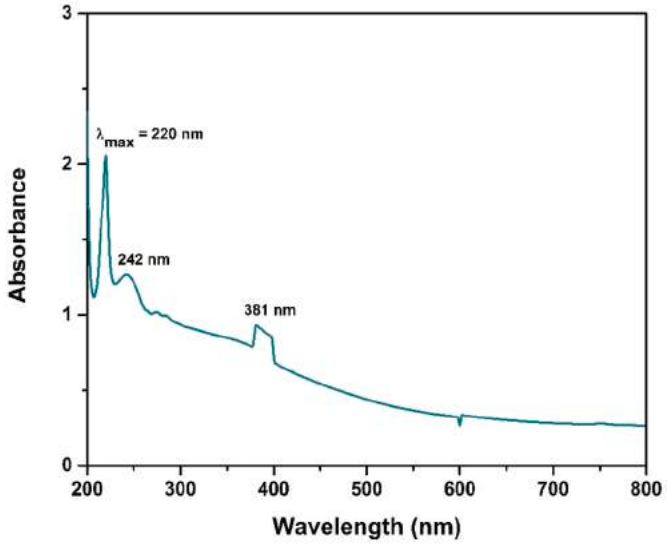

Fig. 6. UV–Vis spectrum of *Averrhoa carambola* L. extract mediated synthesized CuO NPs.

vibrational peaks present within the wavenumber range of 615-621 cm^{-1} which eliminates the possibility of the formation of Cu_2O [74]. The stretching vibrations at 871, 941 and 985 cm^{-1} corresponds to the C–O bonds [69].

3.5. UV–Vis spectroscopic analysis

The optical properties of the *Averrhoa carambola* L. extract mediated synthesized CuO NPs was carried out by UV–Vis spectroscopic analysis (Fig. 6). Such analysis is also a way of confirming the formation of nanoparticles because of the phenomena named surface plasmon resonance (SPR). According to the basic understanding of SPR, when photon interects with the conduction band electrons of the metal/metal oxide nanoparticles, it begets a resonance effect [77,78]. This resonance effect only occurs when the frequency of the incident photons matches with that of the surface electrons [79]. Since the properties of nanoparticles differes from bulk materials, UV–Vis spectroscopic analysis helps in differentiating between them in terms of SPR. The UV–Vis spectrum of CuO NPs shows a sharp absorption peak at 220 nm along with two smaller peaks at 242 and 381 nm respectively. The apex at 220 nm was also reported in previous literature [80–82] and values of other peaks are also consistent with reported literatures [71,83,84].

3.6. Particle size and zeta potential analysis

The particle size of the synthesized CuO NPs was measured by DLS analyzer which implemented the Multi Angle Dynamic Light Scattering (MADLS) technology for better measurement of the particle size. The particle size distribution of CuO NPs is shown in Fig. 7a.

The most prevailing particle sizes were seen to be within 100–150 nm range with the calculated average particle size of 117 nm which is slightly higher than the particle size calculated from FESEM analysis. Two factors might be responsible for such phenomena, one may be due to the agglomeration of particles in the aqueous solution [85] and letter is due to the hydrodynamic diameter of the NPs that are being counted by the DLS particle size analyzer [58]. Particles at smaller sizes (20–50 nm) were also observed but in lesser magnitude. This might be the reason for the multiple peaks that were observed in the SPR spectrum of the CuO NPs (Fig. 6). The obtained polydispersity index (PDI) of 0.5815 is also indicative of the less monodispersity of the synthesized CuO NPs. The stability of the obtained nanoparticles was measured by the zeta potential analysis which is shown in Fig. 7b. The measured zeta potential of CuO NPs at neutral pH was found to be −13.65 mV. The negative value is attributed due to the formation of OH^- groups that forms on the surface of the nanoparticles when dispersed in the aqueous solution [58]. The magnitude of zeta potential (−13.65 mV) signifies the possible agglomeration of the particles due to Van Der Waals interparticle attraction [86] which was also evident from the FESEM images.

3.7. Antibacterial activity of CuO NPs

The antibacterial activity of the synthesized CuO NPs was evaluated in vitro against broad spectrum gram positive and gram negative bacterial strains with reference to broad spectrum antibiotic Kanamycin (30 μg disk) and has been shown in Fig. 8.

Zone of inhibition was recorded after 24 h of incubation for 100 μg/mL concentration of CuO NPs against 3 gram negative bacteria (*Escherichia coli*, *Salmonella typhi and Pseudomonas aeruginosa*) and 2 gram positive bacteria (*Bacillus megaterium* and *Staphylococcus aureus*). Clear zone of inhibition was observed for both the gram positive and gram negative bacteria. The gram negative bacteria were more sensitive to the biosynthesized CuO NPs compared to gram positive bacteria and *Salmonella typhi* was the most susceptible (26 mm) to CuO NPs. *Escherichia coli* was also susceptible (24 mm) and *Pseudomonas aeruginosa* was the least susceptible one (16 mm) among them. *Bacillus megaterium* and *Staphylococcus aureus* had the zone of inhibition of 20 mm and 16 mm

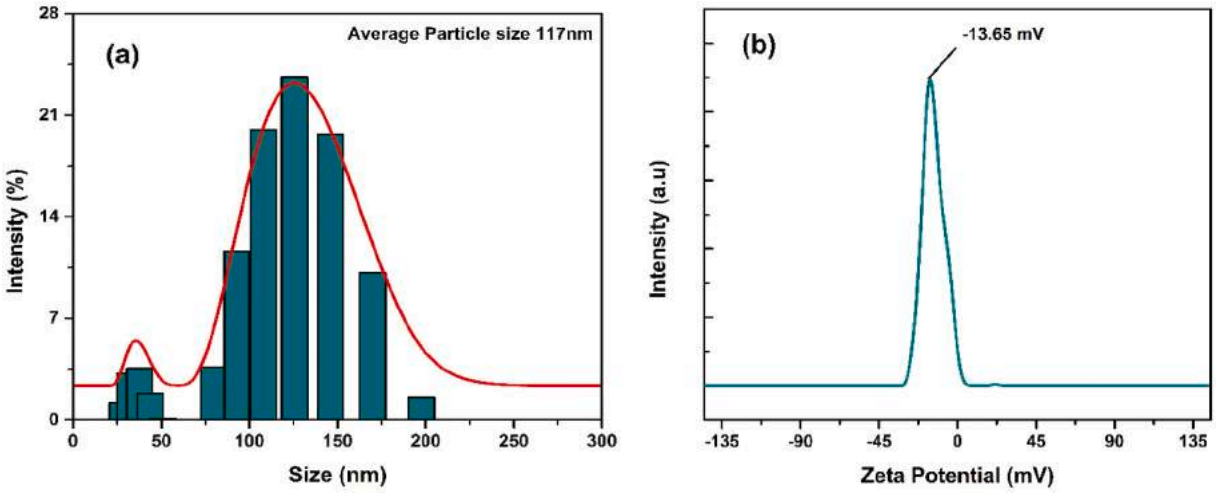

Fig. 7. (a) DLS particle size and (b) zeta potential of the synthesized CuO NPs.

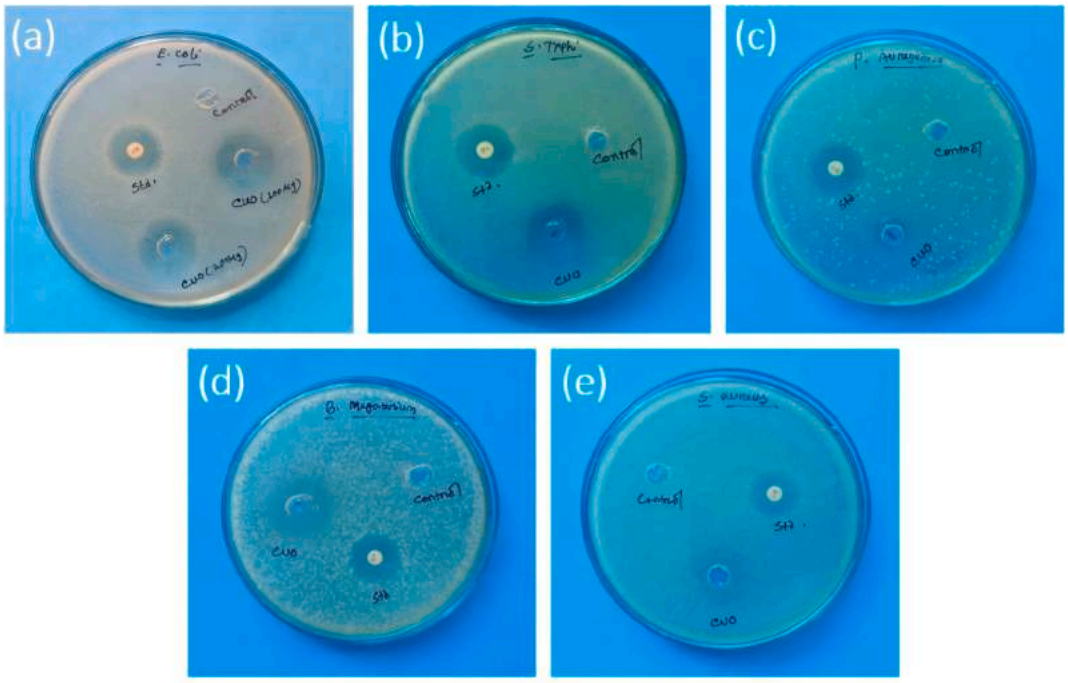

Fig. 8. Agar well diffusion measurements of CuO NPs against (a) *Escherichia coli,* (b) *Salmonella typhi,* (c) *Pseudomonas aeruginosa,* (d) *Bacillus megaterium and* (e) *Staphylococcus aureus*.

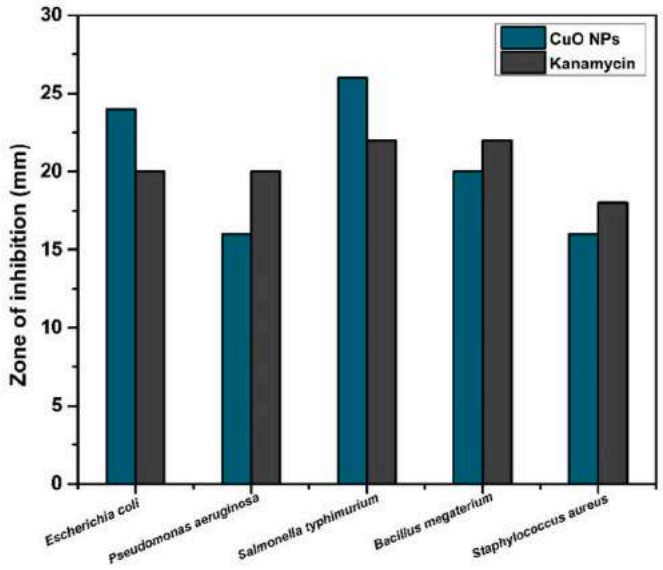

Fig. 9. Comparative antibacterial activity of CuO NPs and broad spectrum antibiotic Kanamycin against 3 gram negative and 2 gram positive bacteria.

respectively. This also carries good evidence of antibacterial efficacy of *Averrhoa carambola* L. extract mediated green synthesized CuO NPS against gram positive bacteria. Fig. 9 shows the comparative antibacterial results of CuO NPs and broad spectrum antibiotic Kanamycin.

3.8. MIC and MBC study

Minimum inhibitory concentration is the lowest concentration at which antimicrobial agent show bacteriostatic activity. The MIC of CuO NPs was determined for 3 gram (ve-) bacteria and 2 gram (ve+) bacteria (Table 2). The concentration of CuO NPs was chosen from 6.25 μg/mL to 100 μg/mL. According to the results, 50 μg/mL concentration of CuO NPs was found to be effective against all the selected bacterial strains and thus, the MIC of *Averrhoa carambola* extract mediated green synthesized CuO NPs is reported to be of 50 μg/mL.

Table 2
MIC results of *Averrhoa carambola* extract mediated green synthesized CuO NPS.

Bacterial Strains	100 μg/mL	50 μg/mL	25 μg/mL	12.5 μg/mL	6.25 μg/mL
Escherichia coli	-	-	-	-	-
Pseudomonas aeruginosa	-	-	-	-	+
Salmonella typhi	-	-	-	+	+
Bacillus megaterium	-	-	-	+	+
Staphylococcus aureus	-	-	+	+	+

*Note: '+' indicates presence of bacterial growth; '-' indicates No bacterial growth.

MBC is the lowest concentration of antimicrobial agent which is bactericidal. For the detection of MBC, concentration of 6.25 μg/mL-100 μg/mL of CuO NPs was considered. After 24 h incubation period, the concentration which did not show any bacterial colony would be described as MBC (Table 3). According to the results, 100 μg/mL concentration of biosynthesized CuO NPs was bactericidal for all selected

Table 3
MBC results of *Averrhoa carambola* extract mediated green synthesized CuO NPS.

Bacterial Strains	100 μg/mL	50 μg/mL	25 μg/mL	12.5 μg/mL	6.25 μg/mL
Escherichia coli	-	-	-	-	-
Pseudomonas aeruginosa	-	-	-	+	+
Salmonella typhi	-	-	+	+	+
Bacillus megaterium	-	-	+	+	+
Staphylococcus aureus	-	+	+	+	+

*Note: '+' indicates presence of bacterial growth; '-' indicates No bacterial growth.

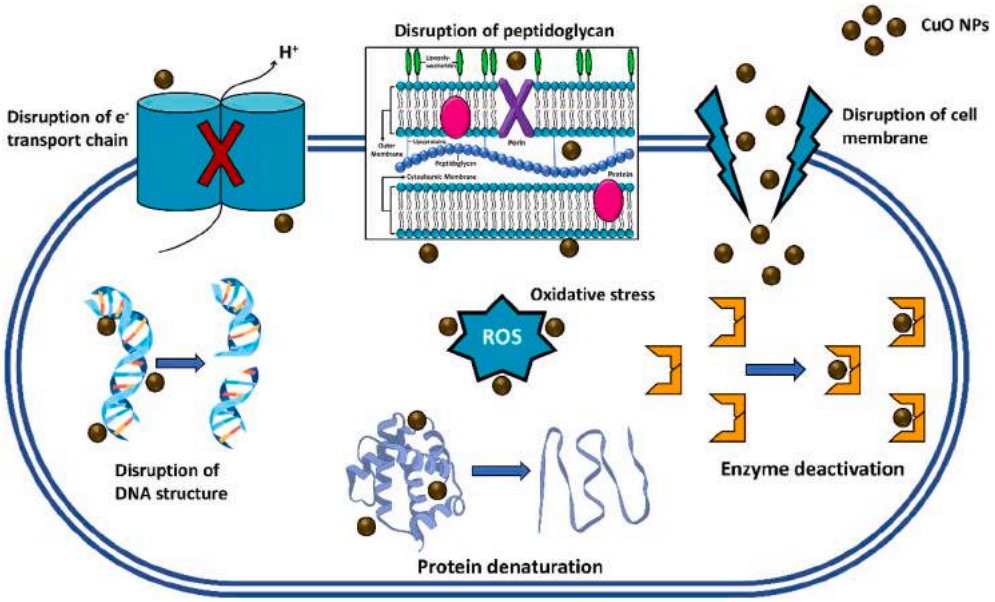

Fig. 10. Visual representation of bactericidal action of CuO NPs.

microbial strains and referred as MBC.

3.9. Mechanism of antibacterial activity and comparative study

The synthesized CuO NPs have been found to be highly active against gram negative bacteria. Several studies also claimed the highest antibacterial activity against gram negative bacteria [34,87–89]. This might be due to the fact that gram negative bacteria has comparatively thin peptidoglycan cell wall surrounded by lipopolysaccharide containing outer membrane, allowing facile perforation of NPs and thus leads to cell death [90]. Although the exact reason behind the high antibacterial activity of CuO NPs hasn't been well established yet but there are some venerable mechanisms which explains the phenomena [13]. The superior activity of CuO NPs may be attributed to the release of Cu ion (Cu^{2+}) from CuO NPs [91,92] which has high affinity towards negative charge of bacterial cell wall by electrostatic forces as well as Van der Waals forces [93]. As a result, it presents adhesive behavior and destroy the cell membrane integrity leading to cell death by sabotaging enzyme activity and promoting cell permeability [88,94]. The generated Cu^{2+} enters the cell and induces cross linkage within the nucleic acid of DNA molecules of bacteria. It consequences the distorted helical structure of DNA causing protein denaturation, interrupted metabolic processes and complete eradication of cell wall of bacteria [42]. Velsankar et al. [68] reported the reaction as well as the mechanism of liberation Cu^{2+} shown as follows:

$$CuO + H_2O \leftrightarrow Cu^{2+} + 2OH^- \quad (8)$$

This reaction proceeds with the following mechanism:

$$CuO + h\vartheta \rightarrow e^- + h^+ \quad (9)$$

$$e^- + O_2 \rightarrow O_2^{-*} \quad (10)$$

$$h^+ + H_2O \rightarrow OH^- + H^+ \quad (11)$$

$$O_2^{-*} + H^+ \rightarrow HO_2^* \quad (12)$$

$$HO_2^* + H^+ \rightarrow H_2O_2 \quad (13)$$

In addition, CuO NPs generate reactive oxygen species such as superoxide radical (O^{-2}), hydroxyl radical (-OH), hydrogen peroxide (H_2O_2), and singlet oxygen (O_2), cascades of reactive oxygen species (ROS) by oxidative stress in the cell resulting protein oxidation, lipid peroxidation, DNA deterioration and cell necrosis [7,87]. Visual representation of the mechanism of antibacterial activity of CuO NPs is shown in Fig. 10.

Biosynthesized CuO NPs have been exploited against various gram positive and gram negative bacteria and few of these reports have been tabulated in Table 4 along with the results of present study.

4. Conclusion

In this study, successful synthesis of CuO NPs was reported employing the leaf extract of *Averrhoa carambola*. The use of such plant extract made the process ecologically sound and cost-effective. Agar well diffusion method was followed for investigating the antibacterial activity of CuO NPs. The sublime bactericidal activity of the bio-resource based green synthesized CuO NPs against both gram (+)ve and gram(−)ve bacterial strains can induce a new horizon for designing potential antimicrobial drug.

Funding

Not applicable.

CRediT authorship contribution statement

Trissa Saha: collected the raw materials, carried out synthesis and wrote draft partially. **Mashrafi Bin Mobarak:** conceived the idea, supervised the work, wrote and finalized the manuscript. **Md Najem Uddin:** carried out the antibacterial experiments. **Md Saiful Quddus:** carried out the XPS analysis. **Mustafizur Rahman Naim:** carried out FESEM and EDX analysis. **Nigar Sultana Pinky:** helped with UV–Vis analysis. All the authors discussed the results and contributed to the writing of the manuscript. All authors have read and agreed to the published version of the manuscript.

Declaration of competing interest

The authors declare that they have no known competing financial interests or personal relationships that could have appeared to influence the work reported in this paper.

Table 4
Antibacterial activity of biosynthesized CuO NPs against various bacteria.

Biological source	Precursor	Bacterial Entity	Zone of Inhibition	Test method	Ref.
Catha edulis leaf extract	Copper (II) nitrate trihydrate	*K. pneumonia*	22 mm	Disc diffusion	[95]
		E. coli	24 mm		
		S. aures	32 mm		
		S. pyogenes	29 mm		
Caesalpinia bonducella seed extract	Copper (II) nitrate trihydrate	*S. aureus*	25 mm	Agar well diffusion	[71]
		Aeromonas sp.	34 mm		
Allium sativum extract	Copper (II) nitrate trihydrate	*Escherichia coli*	11.65 mm	Disk diffusion	[68]
		S. aureus	11.30 mm		
		Bacillus Subtilis	10.90 mm		
		Streptococcus phogenes	10.65 mm		
		Pseudomonas aeruginosa	10.90 mm		
		Klebsiella pheumoniae	10.65 mm		
Cissus Quadrangularis leaf extract	Copper(II) sulfate	*Staphylococcus aureus*	11 mm	Disk diffusion	[96]
		Streptococcus sp.	26 mm		
		Seratia marscenes	20 mm		
Bacopa monnieri leaf extract	Copper (II) acetate monohydrate	*H.salomonis,*	13.50 mm	Agar well diffusion	[11]
		H. felis	15.71 mm		
		H. suis	15.84 mm		
		H. bizzozeronii	13.11 mm		
Aerva Javanica leaf extract	Copper (II) chloride dihydrate	*Escherichia coli*	7 mm	Agar well diffusion	[50]
		Pseudomonas aeruginosa	13 mm		
		Staphylococcus aureus	12 mm		
		Acinetobacter	12 mm		
Carica papaya leaf extract	Copper (II) sulfate	*Escherichia coli*	25 mm	Agar well diffusion	[87]
		B.subtilis	23 mm		
		Staphylococcus aureus	18 mm		
Aloe vera leaf Extract	Copper (II) nitrate	*A. hydrophila,*	21 mm	Agar well diffusion	[42]
		P. fluorescens	19 mm		
		F.branchiophilum (Fish pathogen)	17 mm		
Syzygium alternifolium stem bark	Copper (II) sulfate pentahydrate	*B. subtilis*	~7 mm	Disk diffusion	[94]
		S. aureus,	~8 mm		
		E. coli	~16 mm		
		K. pneumonia	~9 mm		
		P. vulgaris	~8.5 mm		
		P. aeruginosa	~8 mm		
		S. typhimurium	~7 mm		
Achillea Nobilis flowering branch extract	Copper (II) sulfate pentahydrate	*Staphylococcus aureus*	12.2 mm	Agar well diffusion	[97]
		Escherichia coli	9.7 mm		
Punica granatum peel extract	Copper (II) acetate monohydrate	*Escherichia coli*	20 mm	Disk diffusion	[34]
Justicia gendarussa leaf extract	Copper (II) sulfate	*Staphylococcus aureus*	16 mm	Agar well diffusion	[98]
		Escherichia coli	18 mm		
Averrhoa carambola leaf extract	Copper (II) sulfate pentahydrate	*Escherichia coli*	24 mm	Agar well diffusion	*this study
		Pseudomonas aeruginosa	16 mm		
		Salmonella typhi	26 mm		
		Bacillus megaterium	20 mm		
		Staphylococcus aureus	16 mm		

Data availability

Data will be made available on request.

Acknowledgement

We are gratefully acknowledging the support from IGCRT and IFRD, BCSIR (R&D approval ref. 39.02.0000.011.14.134.2021/900; Date: December 30, 2021). We are thankful to Md. Sahadat Hossain and Monika Mahmud for their support with XRD, DLS and zeta (ζ)-potential measurements. We also appreciate Dr. Shirin Akter Jahan for her support with SIGCRT instruments.

References

[1] P.M. Hawkey, The growing burden of antimicrobial resistance, J. Antimicrob. Chemother. 62 (2008) i1–i9.
[2] R. Dadi, R. Azouani, M. Traore, C. Mielcarek, A. Kanaev, Antibacterial activity of ZnO and CuO nanoparticles against gram positive and gram negative strains, Mater. Sci. Eng. C 104 (2019), 109968.
[3] B. Das, S. Moumita, S. Ghosh, M.I. Khan, D. Indira, R. Jayabalan, S.K. Tripathy, A. Mishra, P. Balasubramanian, Biosynthesis of magnesium oxide (MgO) nanoflakes by using leaf extract of Bauhinia purpurea and evaluation of its antibacterial property against Staphylococcus aureus, Mater. Sci. Eng. C 91 (2018) 436–444.
[4] K. Hiramatsu, Vancomycin-resistant Staphylococcus aureus: a new model of antibiotic resistance, Lancet Infect. Dis. 1 (2001) 147–155.
[5] P.S. Umoren, D. Kavaz, A. Nzila, S.S. Sankaran, S.A. Umoren, Biogenic synthesis and characterization of Chitosan-CuO nanocomposite and evaluation of antibacterial activity against gram-positive and-negative bacteria, Polymers 14 (2022) 1832.
[6] M.N. Alekshun, S.B. Levy, Molecular mechanisms of antibacterial multidrug resistance, Cell 128 (2007) 1037–1050.
[7] H. Qamar, A. Saeed, M. Owais, T. Hussain, K. Hussain, A.U. Rahman, S. Ahmed, S. Kumar, Z.A. Khan, CuO bionanocomposite with enhanced stability and antibacterial activity against extended-spectrum beta-lactamase strains, Materials 14 (2021) 6336.
[8] N. Osman, N. Devnarain, C.A. Omolo, V. Fasiku, Y. Jaglal, T. Govender, Surface modification of nano-drug delivery systems for enhancing antibiotic delivery and activity, Wiley Interdiscip. Rev. Nanomed. Nanobiotechnol. 14 (2022) e1758.
[9] D. Mott, J. Galkowski, L. Wang, J. Luo, C.-J. Zhong, Synthesis of size-controlled and shaped copper nanoparticles, Langmuir 23 (2007) 5740–5745.
[10] G.V. Vimbela, S.M. Ngo, C. Fraze, L. Yang, D.A. Stout, Antibacterial properties and toxicity from metallic nanomaterials, Int. J. Nanomed. 12 (2017) 3941.
[11] S. Faisal, H. Jan, Abdullah, I. Alam, M. Rizwan, Z. Hussain, K. Sultana, Z. Ali, M. N. Uddin, In vivo analgesic, anti-inflammatory, and anti-diabetic screening of Bacopa monnieri-synthesized copper oxide nanoparticles, ACS Omega 7 (2022) 4071–4082.
[12] E. Sánchez-López, D. Gomes, G. Esteruelas, L. Bonilla, A.L. Lopez-Machado, R. Galindo, A. Cano, M. Espina, M. Ettcheto, A. Camins, Metal-based nanoparticles as antimicrobial agents: an overview, Nanomaterials 10 (2020) 292.

[13] P.G. Bhavyasree, T.S. Xavier, Green synthesised copper and copper oxide based nanomaterials using plant extracts and their application in antimicrobial activity, Curr. Res. Green Sustain. Chem. 5 (2022), 100249.
[14] A.C. Janaki, E. Sailatha, S. Gunasekaran, Synthesis, characteristics and antimicrobial activity of ZnO nanoparticles, Spectrochim. Acta. A. Mol. Biomol. Spectrosc. 144 (2015) 17–22.
[15] S. Yadav, G. Jaiswar, Review on undoped/doped TiO2 nanomaterial; synthesis and photocatalytic and antimicrobial activity, J. Chin. Chem. Soc. 64 (2017) 103–116.
[16] S.V. Gudkov, D.A. Serov, M.E. Astashev, A.A. Semenova, A.B. Lisitsyn, Ag2O nanoparticles as a candidate for antimicrobial compounds of the new generation, Pharmaceuticals 15 (2022) 968.
[17] M.A. Ansari, H.M. Khan, A.A. Khan, R. Pal, S.S. Cameotra, Antibacterial potential of Al2O3 nanoparticles against multidrug resistance strains of Staphylococcus aureus isolated from skin exudates, J. Nanoparticle Res. 15 (2013) 1–12.
[18] F. Mukhtar, T. Munawar, M.S. Nadeem, S.A. Khan, M. Koc, S. Batool, M. Hasan, F. Iqbal, Enhanced sunlight-absorption of Fe2O3 covered by PANI for the photodegradation of organic pollutants and antimicrobial inactivation, Adv. Powder Technol. 33 (2022), 103708.
[19] B. Ahmad, M.I. Khan, M.A. Naeem, A. Alhodaib, M. Fatima, M. Amami, E.A. Al-Abbad, A. Kausar, N. Alwadai, A. Nazir, Green synthesis of NiO nanoparticles using Aloe vera gel extract and evaluation of antimicrobial activity, Mater. Chem. Phys. (2022), 126363.
[20] W. Ahmad, A. Kamboj, I. Banerjee, K.K. Jaiswal, Pomegranate peels mediated synthesis of calcium oxide (CaO) nanoparticles, characterization, and antimicrobial applications, Inorg. Nano-Met. Chem. (2022) 1–8.
[21] B.K. Sharma, B.R. Mehta, V.P. Chaudhari, E.V. Shah, S. Mondal Roy, D.R. Roy, Green synthesis of dense rock MgO nanoparticles using carica papaya leaf extract and its shape dependent antimicrobial activity: joint Experimental and DFT Investigation, J. Cluster Sci. 33 (2022) 1667–1675.
[22] M.S. Al-Fakeh, R.O. Alsaedi, Synthesis, characterization, and antimicrobial activity of CoO nanoparticles from a Co (II) complex derived from polyvinyl alcohol and aminobenzoic acid derivative, Sci. World J. 2021 (2021).
[23] R. Venkatesan, N. Rajeswari, Preparation, mechanical and antimicrobial properties of SiO2/poly (butylene adipate-co-terephthalate) films for active food packaging, Silicon 11 (2019) 2233–2239.
[24] B. Peng, C. Feng, S. Liu, R. Zhang, Synthesis of CuO catalyst derived from HKUST-1 temple for the low-temperature NH3-SCR process, Catal. Today 314 (2018) 122–128.
[25] P. Rana, S. Gupta, I. Pop, G. Gupta, Three-dimensional heat transfer of 29 nm CuO-H2O nanoliquid with Joule heating and slip effects over a wedge surface, Int. Commun. Heat Mass Tran. 134 (2022), 106001.
[26] H. Purnama, T. Ressler, R.E. Jentoft, H. Soerijanto, R. Schlögl, R. Schomäcker, CO formation/selectivity for steam reforming of methanol with a commercial CuO/ZnO/Al2O3 catalyst, Appl. Catal. Gen. 259 (2004) 83–94.
[27] J.-L. Cao, G.-S. Shao, Y. Wang, Y. Liu, Z.-Y. Yuan, CuO catalysts supported on attapulgite clay for low-temperature CO oxidation, Catal. Commun. 9 (2008) 2555–2559.
[28] C.-Y. Chiang, K. Aroh, N. Franson, V.R. Satsangi, S. Dass, S. Ehrman, Copper oxide nanoparticle made by flame spray pyrolysis for photoelectrochemical water splitting–Part II. Photoelectrochemical study, Int. J. Hydrogen Energy 36 (2011) 15519–15526.
[29] Y. She, Q. Zheng, L. Li, Y. Zhan, C. Chen, Y. Zheng, X. Lin, Rare earth oxide modified CuO/CeO2 catalysts for the water–gas shift reaction, Int. J. Hydrogen Energy 34 (2009) 8929–8936.
[30] M. Frietsch, F. Zudock, J. Goschnick, M. Bruns, CuO catalytic membrane as selectivity trimmer for metal oxide gas sensors, Sensor. Actuator. B Chem. 65 (2000) 379–381.
[31] F. Jiang, B. Ding, Y. Zhao, S. Liang, Z. Cheng, B. Xing, B. Teng, P. Ma, J. Lin, Biocompatible CuO-decorated carbon nanoplatforms for multiplexed imaging and enhanced antitumor efficacy via combined photothermal therapy/chemodynamic therapy/chemotherapy, Sci. China Mater. 63 (2020) 1818–1830.
[32] S. Yallappa, J. Manjanna, M.A. Sindhe, N.D. Satyanarayan, S.N. Pramod, K. Nagaraja, Microwave assisted rapid synthesis and biological evaluation of stable copper nanoparticles using T. arjuna bark extract, Spectrochim. Acta. A. Mol. Biomol. Spectrosc. 110 (2013) 108–115.
[33] O. Lupan, V. Postica, V. Cretu, N. Wolff, V. Duppel, L. Kienle, R. Adelung, Single and networked CuO nanowires for highly sensitive p-type semiconductor gas sensor applications, Phys. Status Solidi RRL 10 (2016) 260–266.
[34] V.U. Siddiqui, A. Ansari, R. Chauhan, W.A. Siddiqi, Green synthesis of copper oxide (CuO) nanoparticles by Punica granatum peel extract, Mater. Today Proc. 36 (2021) 751–755.
[35] H.N. Cuong, S. Pansambal, S. Ghotekar, R. Oza, N.T.T. Hai, N.M. Viet, V.-H. Nguyen, New frontiers in the plant extract mediated biosynthesis of copper oxide (CuO) nanoparticles and their potential applications: a review, Environ. Res. (2021), 111858.
[36] S. Iravani, Green synthesis of metal nanoparticles using plants, Green Chem. 13 (2011) 2638–2650.
[37] A. Raja, S. Ashokkumar, R.P. Marthandam, J. Jayachandiran, C.P. Khatiwada, K. Kaviyarasu, R.G. Raman, M. Swaminathan, Eco-friendly preparation of zinc oxide nanoparticles using Tabernaemontana divaricata and its photocatalytic and antimicrobial activity, J. Photochem. Photobiol., B 181 (2018) 53–58.
[38] J. Singh, V. Kumar, K.-H. Kim, M. Rawat, Biogenic synthesis of copper oxide nanoparticles using plant extract and its prodigious potential for photocatalytic degradation of dyes, Environ. Res. 177 (2019), 108569.
[39] S. Prabhu, E.K. Poulose, Silver nanoparticles: mechanism of antimicrobial action, synthesis, medical applications, and toxicity effects, Int. Nano Lett. 2 (2012) 1–10.
[40] P. Narasaiah, B.K. Mandal, N.C. Sarada, Biosynthesis of copper oxide nanoparticles from Drypetes sepiaria leaf extract and their catalytic activity to dye degradation, in: IOP Conf. Ser. Mater. Sci. Eng., IOP Publishing, 2017, 022012.
[41] N. Sebeia, M. Jabli, A. Ghith, Biological synthesis of copper nanoparticles, using Nerium oleander leaves extract: characterization and study of their interaction with organic dyes, Inorg. Chem. Commun. 105 (2019) 36–46.
[42] P.P.N. Kumar, U. Shameem, P. Kollu, R.L. Kalyani, S.V.N. Pammi, Green synthesis of copper oxide nanoparticles using Aloe vera leaf extract and its antibacterial activity against fish bacterial pathogens, BioNanoScience 5 (2015) 135–139.
[43] K. Vishveshvar, A. Krishnan, K. Haribabu, S. Vishnuprasad, Green synthesis of copper oxide nanoparticles using Ixiro coccinea plant leaves and its characterization, BioNanoScience 8 (2018) 554–558.
[44] Z. Alhalili, Green synthesis of copper oxide nanoparticles CuO NPs from Eucalyptus Globoulus leaf extract: adsorption and design of experiments, Arab. J. Chem. 15 (2022), 103739.
[45] R. Katwal, H. Kaur, G. Sharma, M. Naushad, D. Pathania, Electrochemical synthesized copper oxide nanoparticles for enhanced photocatalytic and antimicrobial activity, J. Ind. Eng. Chem. 31 (2015) 173–184.
[46] S.-D. Wei, H. Chen, T. Yan, Y.-M. Lin, H.-C. Zhou, Identification of antioxidant components and fatty acid profiles of the leaves and fruits from Averrhoa carambola, LWT-Food Sci. Technol. 55 (2014) 278–285.
[47] K. Lakmal, P. Yasawardene, U. Jayarajah, S.L. Seneviratne, Nutritional and medicinal properties of Star fruit (Averrhoa carambola): a review, Food Sci. Nutr. 9 (2021) 1810–1823.
[48] S.W. Yan, R. Ramasamy, N.B.M. Alitheen, A. Rahmat, A comparative assessment of nutritional composition, total phenolic, total flavonoid, antioxidant capacity, and antioxidant vitamins of two types of Malaysian underutilized fruits (Averrhoa bilimbi and Averrhoa carambola), Int. J. Food Prop. 16 (2013) 1231–1244.
[49] C. Perez, Antibiotic assay by agar-well diffusion method, Acta Biol. Med. Exp. 15 (1990) 113–115.
[50] F. Amin, B. Khattak, A. Alotaibi, M. Qasim, I. Ahmad, R. Ullah, M. Bourhia, A. Gul, S. Zahoor, R. Ahmad, Green synthesis of copper oxide nanoparticles using Aerva javanica leaf extract and their characterization and investigation of in vitro antimicrobial potential and cytotoxic activities, Evid. Based Complement, Alternative Med. 2021 (2021).
[51] I. Wiegand, K. Hilpert, R.E. Hancock, Agar and broth dilution methods to determine the minimal inhibitory concentration (MIC) of antimicrobial substances, Nat. Protoc. 3 (2008) 163–175.
[52] S. Prakash, N. Elavarasan, A. Venkatesan, K. Subashini, M. Sowndharya, V. Sujatha, Green synthesis of copper oxide nanoparticles and its effective applications in Biginelli reaction, BTB photodegradation and antibacterial activity, Adv. Powder Technol. 29 (2018) 3315–3326.
[53] P. Vinothkumar, C. Manoharan, B. Shanmugapriya, M. Bououdina, Effect of reaction time on structural, morphological, optical and photocatalytic properties of copper oxide (CuO) nanostructures, J. Mater. Sci. Mater. Electron. 30 (2019) 6249–6262.
[54] M. Amiri, H.A. Javar, H. Mahmoudi-Moghaddam, M. Salavati-Niasari, Green synthesis of perovskite-type nanocomposite using Crataegus for modification of bisphenol a sensor, Microchem. J. 178 (2022), 107411.
[55] J. Baneshi, M. Haghighi, N. Jodeiri, M. Abdollahifar, H. Ajamein, Homogeneous precipitation synthesis of CuO–ZrO2–CeO2–Al2O3 nanocatalyst used in hydrogen production via methanol steam reforming for fuel cell applications, Energy Convers. Manag. 87 (2014) 928–937.
[56] M. Hossain, M. Hasan, M. Mahmud, M.B. Mobarak, S. Ahmed, Assessment of crystallite size of UV-synthesized hydroxyapatite using different model equations, Chem. Pap. (2022) 1–9.
[57] P. Scherrer, Bestimmung der inneren Struktur und der Größe von Kolloidteilchen mittels Röntgenstrahlen, in: Kolloidchem. Ein Lehrb., Springer, 1912, pp. 387–409.
[58] M.B. Mobarak, M.S. Hossain, F. Chowdhury, S. Ahmed, Synthesis and characterization of CuO nanoparticles utilizing waste fish scale and exploitation of XRD peak profile analysis for approximating the structural parameters, Arab. J. Chem. 15 (2022), 104117.
[59] M. Hossain, M. Mahmud, M.B. Mobarak, S. Ahmed, Crystallographic analysis of biphasic hydroxyapatite synthesized by different methods: an appraisal between new and existing models, Chem. Pap. (2021) 1–13.
[60] S.K. Shinde, D.P. Dubal, G.S. Ghodake, V.J. Fulari, Hierarchical 3D-flower-like CuO nanostructure on copper foil for supercapacitors, RSC Adv. 5 (2015) 4443–4447.
[61] S. Ahmad, S.B. Khan, A.M. Asiri, H.M. Marwani, T. Kamal, Polypeptide and copper oxide nanocomposite hydrogel for toxicity elimination of wastewater, J. Sol. Gel Sci. Technol. 96 (2020) 382–394.
[62] K.P. Sapkota, I. Lee, M.A. Hanif, M.A. Islam, J. Akter, J.R. Hahn, Enhanced visible-light photocatalysis of nanocomposites of copper oxide and single-walled carbon nanotubes for the degradation of methylene blue, Catalysts 10 (2020) 297.
[63] A.S. Ethiraj, D.J. Kang, Synthesis and characterization of CuO nanowires by a simple wet chemical method, Nanoscale Res. Lett. 7 (2012) 1–5.
[64] C. Chen, X. Liu, Q. Fang, X. Chen, T. Liu, M. Zhang, Self-assembly synthesis of CuO/ZnO hollow microspheres and their photocatalytic performance under natural sunlight, Vacuum 174 (2020), 109198.
[65] A. Molazemhosseini, L. Magagnin, P. Vena, C.-C. Liu, Single-use nonenzymatic glucose biosensor based on CuO nanoparticles ink printed on thin film gold electrode by micro-plotter technology, J. Electroanal. Chem. 789 (2017) 50–57.
[66] M.A. Khan, N. Nayan, M.K. Ahmad, C.F. Soon, Surface study of CuO nanopetals by advanced nanocharacterization techniques with enhanced optical and catalytic properties, Nanomaterials 10 (2020) 1298.

[67] R. Chowdhury, A. Khan, M.H. Rashid, Green synthesis of CuO nanoparticles using Lantana camara flower extract and their potential catalytic activity towards the aza-Michael reaction, RSC Adv. 10 (2020) 14374–14385.
[68] K. Velsankar, A.K. Rm, R. Preethi, V. Muthulakshmi, S. Sudhahar, Green synthesis of CuO nanoparticles via Allium sativum extract and its characterizations on antimicrobial, antioxidant, antilarvicidal activities, J. Environ. Chem. Eng. 8 (2020), 104123.
[69] P. Bhattacharya, S. Swarnakar, S. Ghosh, S. Majumdar, S. Banerjee, Disinfection of drinking water via algae mediated green synthesized copper oxide nanoparticles and its toxicity evaluation, J. Environ. Chem. Eng. 7 (2019), 102867.
[70] K. Lakshmi, M. Jayashree, K. Shakila Banu, Green and chemically synthesized copper oxide nanoparticles-A preliminary research towards its toxic behaviour, Int. J. Pharm. Pharmaceut. Sci. 7 (2015) 156–160.
[71] S. Sukumar, A. Rudrasenan, D. Padmanabhan Nambiar, Green-synthesized rice-shaped copper oxide nanoparticles using Caesalpinia bonducella seed extract and their applications, ACS Omega 5 (2020) 1040–1051.
[72] P.M. Mishra, S.K. Sahoo, G.K. Naik, K. Parida, Biomimetic synthesis, characterization and mechanism of formation of stable silver nanoparticles using Averrhoa carambola L. leaf extract, Mater. Lett. 160 (2015) 566–571.
[73] S. Gunalan, R. Sivaraj, R. Venckatesh, Aloe barbadensis Miller mediated green synthesis of mono-disperse copper oxide nanoparticles: optical properties, Spectrochim, Acta. A. Mol. Biomol. Spectrosc. 97 (2012) 1140–1144.
[74] M. Chauhan, B. Sharma, R. Kumar, G.R. Chaudhary, A.A. Hassan, S. Kumar, Green synthesis of CuO nanomaterials and their proficient use for organic waste removal and antimicrobial application, Environ. Res. 168 (2019) 85–95.
[75] T. Pandiyarajan, R. Udayabhaskar, S. Vignesh, R.A. James, B. Karthikeyan, Synthesis and concentration dependent antibacterial activities of CuO nanoflakes, Mater. Sci. Eng. C 33 (2013) 2020–2024.
[76] L. Debbichi, M.C. Marco de Lucas, J.F. Pierson, P. Kruger, Vibrational properties of CuO and Cu4O3 from first-principles calculations, and Raman and infrared spectroscopy, J. Phys. Chem. C 116 (2012) 10232–10237.
[77] J. Jana, M. Ganguly, T. Pal, Enlightening surface plasmon resonance effect of metal nanoparticles for practical spectroscopic application, RSC Adv. 6 (2016) 86174–86211.
[78] C. Rhodes, S. Franzen, J.-P. Maria, M. Losego, D.N. Leonard, B. Laughlin, G. Duscher, S. Weibel, Surface plasmon resonance in conducting metal oxides, J. Appl. Phys. 100 (2006), 054905.
[79] V. Selvamani, Stability studies on nanomaterials used in drugs, in: Charact. Biol. Nanomater. Drug Deliv., Elsevier, 2019, pp. 425–444.
[80] K.B. Manjunatha, R.S. Bhat, A. Shashidhara, H.S. Kumar, S. Nagashree, Antimicrobial and nonlinear optical studies of copper oxide nanoparticles, J. Electron. Mater. 50 (2021) 3415–3421.
[81] P. Singh, K.R. Singh, J. Singh, S.N. Das, R.P. Singh, Tunable electrochemistry and efficient antibacterial activity of plant-mediated copper oxide nanoparticles synthesized by Annona squamosa seed extract for agricultural utility, RSC Adv. 11 (2021) 18050–18060.
[82] D. Rehana, D. Mahendiran, R.S. Kumar, A.K. Rahiman, Evaluation of antioxidant and anticancer activity of copper oxide nanoparticles synthesized using medicinally important plant extracts, Biomed. Pharmacother. 89 (2017) 1067–1077.
[83] A.E.D. Mahmoud, K.M. Al-Qahtani, S.O. Alflaij, S.F. Al-Qahtani, F.A. Alsamhan, Green copper oxide nanoparticles for lead, nickel, and cadmium removal from contaminated water, Sci. Rep. 11 (2021) 1–13.
[84] M.I. Said, A.A. Othman, Structural, optical and photocatalytic properties of mesoporous CuO nanoparticles with tunable size and different morphologies, RSC Adv. 11 (2021) 37801–37813.
[85] R. Shashanka, Investigation of optical and thermal properties of CuO and ZnO nanoparticles prepared by Crocus Sativus (Saffron) flower extract, J. Iran. Chem. Soc. 18 (2021) 415–427.
[86] A.J. Shnoudeh, I. Hamad, R.W. Abdo, L. Qadumii, A.Y. Jaber, H.S. Surchi, S. Z. Alkelany, Synthesis, characterization, and applications of metal nanoparticles, in: Biomater. Bionanotechnol., Elsevier, 2019, pp. 527–612.
[87] B. Turakhia, M.B. Divakara, M.S. Santosh, S. Shah, Green synthesis of copper oxide nanoparticles: a promising approach in the development of antibacterial textiles, J. Coating Technol. Res. 17 (2020) 531–540.
[88] J. Iqbal, A. Andleeb, H. Ashraf, B. Meer, A. Mehmood, H. Jan, G. Zaman, M. Nadeem, S. Drouet, H. Fazal, Potential antimicrobial, antidiabetic, catalytic, antioxidant and ROS/RNS inhibitory activities of Silybum marianum mediated biosynthesized copper oxide nanoparticles, RSC Adv. 12 (2022) 14069–14083.
[89] G.T. Anand, S.J. Sundaram, K. Kanimozhi, R. Nithiyavathi, K. Kaviyarasu, Microwave assisted green synthesis of CuO nanoparticles for environmental applications, Mater, Today Proc 36 (2021) 427–434.
[90] A. Pugazhendhi, S.S. Kumar, M. Manikandan, M. Saravanan, Photocatalytic properties and antimicrobial efficacy of Fe doped CuO nanoparticles against the pathogenic bacteria and fungi, Microb. Pathog. 122 (2018) 84–89.
[91] N.-F. Chen, Y.-H. Liao, P.-Y. Lin, W.-F. Chen, Z.-H. Wen, S. Hsieh, Investigation of the characteristics and antibacterial activity of polymer-modified copper oxide nanoparticles, Int. J. Mol. Sci. 22 (2021), 12913.
[92] A. Nieto-Maldonado, S. Bustos-Guadarrama, H. Espinoza-Gomez, L.Z. Flores-López, K. Ramirez-Acosta, G. Alonso-Nuñez, R.D. Cadena-Nava, Green synthesis of copper nanoparticles using different plant extracts and their antibacterial activity, J. Environ. Chem. Eng. 10 (2022), 107130.
[93] K. Velsankar, V. Vinothini, S. Sudhahar, M.K. Kumar, S. Mohandoss, Green Synthesis of CuO nanoparticles via Plectranthus amboinicus leaves extract with its characterization on structural, morphological, and biological properties, Appl. Nanosci. 10 (2020) 3953–3971.
[94] P. Yugandhar, T. Vasavi, P. Uma Maheswari Devi, N. Savithramma, Bioinspired green synthesis of copper oxide nanoparticles from Syzygium alternifolium (Wt.) Walp: characterization and evaluation of its synergistic antimicrobial and anticancer activity, Appl. Nanosci. 7 (2017) 417–427.
[95] W.W. Andualem, F.K. Sabir, E.T. Mohammed, H.H. Belay, B.A. Gonfa, Synthesis of copper oxide nanoparticles using plant leaf extract of Catha edulis and its antibacterial activity, J. Nanotechnol. 2020 (2020).
[96] S. Rajeshkumar, S. Menon, M. Ponnanikajamideen, D. Ali, K. Arunachalam, Anti-inflammatory and antimicrobial potential of Cissus quadrangularis-assisted copper oxide nanoparticles, J. Nanomater. 2021 (2021).
[97] S.M.E. Sepasgozar, S. Mohseni, B. Feizyzadeh, A. Morsali, Green synthesis of zinc oxide and copper oxide nanoparticles using Achillea Nobilis extract and evaluating their antioxidant and antibacterial properties, Bull. Mater. Sci. 44 (2021) 1–13.
[98] S. Vasantharaj, P. Shivakumar, S. Sathiyavimal, P. Senthilkumar, S. Vijayaram, M. Shanmugavel, A. Pugazhendhi, Antibacterial activity and photocatalytic dye degradation of copper oxide nanoparticles (CuONPs) using Justicia gendarussa, Appl. Nanosci. (2021) 1–8.